Engineering Structures 303 (2024) 117497

Contents lists available at ScienceDirect

Engineering Structures

journal homepage: www.elsevier.com/locate/engstruct

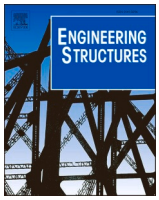

Model for rapid evaluation of corner crack widths in reinforced concrete dapped-end conections

Boyan I. Mihaylov

Department of ArGEnCo, University of Liège, Building B52, Quartier Polytech 1, Allée de la Découverte 9, B-4000 Liège, Belgium

A R T I C L E I N F O

Keywords:
Dapped-end connections
Re-entrant corner crack
Crack width model

A B S T R A C T

Dapped-end connections are widely used in concrete infrastructure, and in particular in Gerber-type bridges and precast concrete buildings. The main vulnerability of such connections is the early opening of inclined cracks at the re-entrant corner of the dapped end. Such cracks are difficult to control as they propagate at low loads and open significantly before the occurrence of secondary cracks. The goal of this paper is to propose a rational model for rapid evaluation of the width of the corner cracks, including the effects of secondary cracking and, indirectly, the effect of restrained shrinkage at low loads. The model assumptions stem from detailed test observations of specimens with light and heavy reinforcement, arranged in orthogonal or diagonal layouts. The model is developed in two steps: 1) predicting the crack width at yielding of the connection, and 2) capturing the shape of the response from zero load up to yielding. A database of 42 tests with a broad range of variables is used to validate the model. It is shown that the main properties influencing the width of the corner crack are the amount and detailing of the reinforcement, and their effect is well captured by the model. It is also illustrated how the model can be used to design the reinforcement of dapped ends to meet crack width limits at service conditions.

1. Introduction

Dapped-end connections are common in concrete bridges and buildings as they provide a compact link between different structural elements. In the past, dapped-ends were widely used in Gerber-type bridges, where they act as hinges in the superstructure – see Fig. 1a. At present, such connections are very common in precast structures of buildings, where they usually link two beams or a beam and a corbel. The main advantage of this connection is its compactness, allowing to maintain a constant total depth of the structure. At the same time, because the depth of the connected elements is abruptly reduced to approximately one-half of their total depth, dapped ends work with complex flow of forces and high stresses in the re-entrant corner.

At ultimate limit state, dapped-end connections are typically designed with strut-and-tie models [1–5]. As shown in Fig. 1b, such models have been developed mainly for two reinforcement layouts: orthogonal and diagonal [6]. In the latter layout, the diagonal reinforcement is typically designed to carry approximately one-half of the total applied shear force ($V_1 \approx V_2$). These models provide safe designs and inform proper detailing of the reinforcement. However, they are not well suited for checks at serviceability limit state. At the same time, dapped ends are very susceptible to wide cracks under service loads.

The main issue at service conditions are inclined cracks that propagate from the re-entrant corner of the connection. Such cracks have been observed in multiple experimental studies [4], [6–12] and field inspections – see Fig. 1a. The corner cracks occur very early due to stress concentration and restrained shrinkage at the re-entrant corner. As a result, the width of the crack often exceeds typical serviceability limits of 0.3–0.4 mm [5]. This often causes durability (and even safety) issues [13–15], as it facilitates the penetration of corrosive agents to the main reinforcement in the re-entrant corner (Fig. 1a). Therefore, it is important to accurately evaluate the width of the cracks in the design process, and to take measures to control them under service loads. However, with the exception of few recommendations [7,16], there is a lack of reliable mechanical models for evaluating re-entrant corner crack widths.

To address this gap, the current study proposes a model for the nonlinear behavior of dapped-end connections in terms of applied shear force versus crack width. The model captures the response from zero load up to yielding of the connection, while at the same time it requires only “hand” calculations with clear physical meaning. The model is validated with detailed crack measurements performed on 42 dapped ends with a wide range of properties, including orthogonal and diagonal reinforcement layouts [4,7,11,12]. The proposed approach is also used to draw recommendations for the design of dapped-end connections at

E-mail address: boyan.mihaylov@uliege.be.

https://doi.org/10.1016/j.engstruct.2024.117497
Received 8 September 2023; Received in revised form 30 November 2023; Accepted 5 January 2024
Available online 13 January 2024

a) Connection in a bridge deck with a re-entrant corner crack and related deterioration (photo courtesy by SPW)

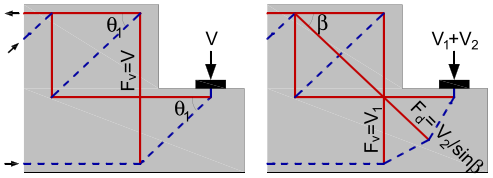

b) Strut-and-tie models for orthogonal and diagonal reinforcement layouts

Fig. 1. Reinforced concrete dapped-end connections.

service conditions.

2. Cracking behavior of dapped-end connections

2.1. Test specimens

To establish the model assumptions, it is instructive to examine the behavior of dapped-end connections observed in tests with detailed crack and deformation measurements. The author and collaborators have performed and reported an experimental program on loading to failure of 16 dapped ends, 8 with orthogonal and 8 with diagonal reinforcement (Rajapakse et al. [11], [12]). The total depth of the specimens was 1000 mm, the depth of the dapped end was 500 mm, and the width of the section was 350 mm. The transverse load (shear force V) was applied on the dapped ends at 320 mm from the re-entrant corner via a steel plate. The compressive strength of the concrete varied slightly around an average value of 51.6 MPa. The geometry and reinforcement of the dapped-ends is illustrated in Fig. 2 using four selected specimens.

In the series with orthogonal reinforcement (OL series), pairs of specimens had identical bottom horizontal reinforcement in the dapped end, but different vertical reinforcement (stirrups) in the vicinity of the re-entrant corner. For each pair, the total area of the stirrups A_{sv} was either ~0.66 or ~1.33 times the area of the horizontal reinforcement A_{sh}. The total amount of reinforcement in the OL series was varied from very light to very heavy, with an approximately four-fold increase of A_{sh}. The bigger area was generally achieved with bigger bar diameters. Table 1 summarizes the main properties of the test specimens, together with the measured ultimate capacity (strength) of the dapped-end connections $V_{u,exp}$.

In the series with diagonal reinforcement (DL series), the horizontal and vertical reinforcement was decreased by ~1/2 as compared to the OL series. Diagonal bars were added to approximately recover the strength of the OL specimens based on simple strut-and-tie considerations. The main properties of the DL series are also summarized in Table 1. All details of the 16 tests are reported elsewhere [11,12].

2.2. Behavior of lightly-reinforced dapped ends

The crack opening behavior of two lightly-reinforced dapped ends is shown in Fig. 3. One of the specimens, OL1, had an orthogonal reinforcement layout, and the other, DL1, had diagonal reinforcement. On the horizontal axis of the plot is the crack width at the re-entrant corner w, and on the vertical axis is the normalized shear force V/V_u (V_u is the ultimate capacity).

The crack patterns of the two specimens at ~50% of the peak load are shown in Fig. 4 (top). The crack width was measured using one horizontal and one vertical displacement transducer as indicated in the crack diagrams. The readings of the two transducers w_h and w_v remained approximately equal throughout the response, and therefore they were combined to obtain w as $\sqrt{(w_h^2 + w_v^2)}$. Several manual crack width measurements from crack comparators are also shown in the cracks

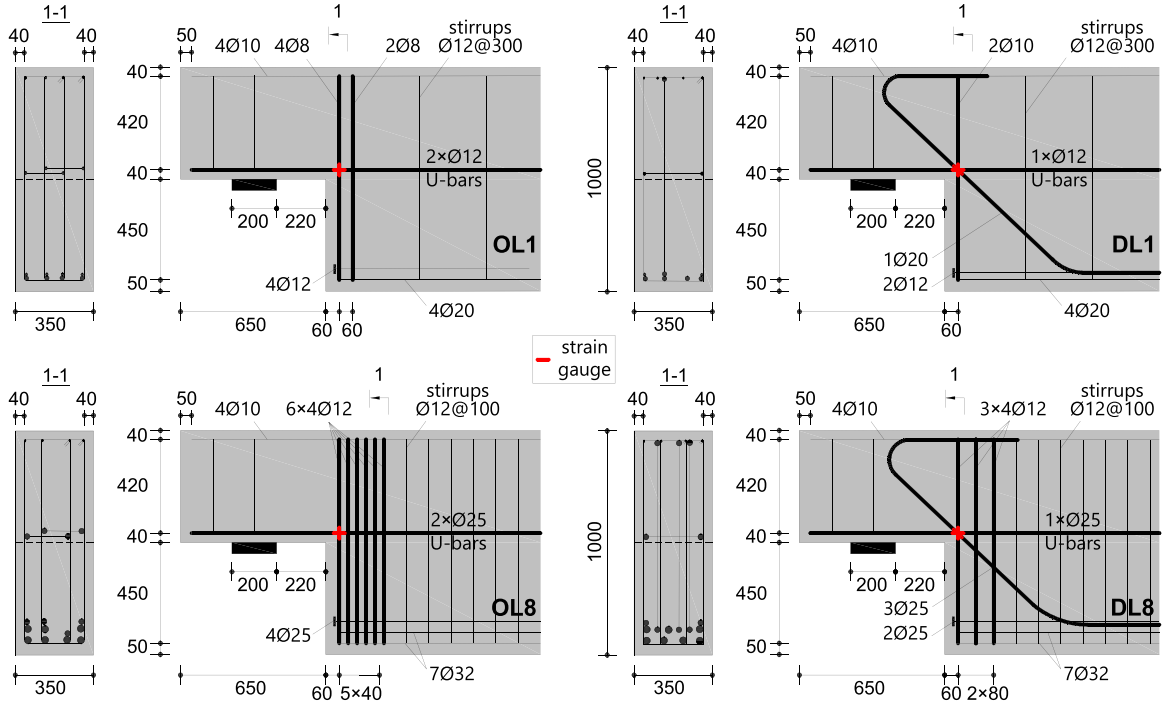

Fig. 2. Selected test specimens from the series by Rajapakse et al. [11,12].

Table 1
Tests of dapped-end connections.

No.	Ref.	Beam name	a (mm)	a_{cl} (mm)	h (mm)	b (mm)	$c_{1,h}$ (mm)	$c_{2,h}$ (mm)	*Hor. bars*	f_{yh} (MPa)	c_v (mm)	*Vert. bars*	f_{yv} (MPa)	c_d (mm)	*Diag. bars*	f_{yd} (MPa)	f_c' (MPa)	$V_{u,exp}$ *T1* (kN)	$V_{u,exp}$ *T2* (kN)	$w_{y,1}$ (mm)	$w_{y,2}$ (mm)	$w_{y,3}$ (mm)	k_{cr} (-)	$w_{y,pred}$ (mm)
1	11,12	1-OL1	320	220	500	350	40	40	$4d_b12$	537	32	$6d_b8$	521	-	-	-	52.1	257	-	**1.61**	1.18	-	0.90	1.61
2		1-OL2	320	220	500	350	40	40	$4d_b12$	537	32	$12d_b8$	521	-	-	-	52.1	299	-	**1.61**	1.04	-	0.90	1.61
3		2-OL3	320	220	500	350	40	40	$4d_b16$	599	30	$8d_b10$	509	-	-	-	51.3	524	-	**2.06**	1.16	-	0.45	2.06
4		2-OL4	320	220	500	350	40	40	$4d_b16$	599	30	$14d_b10$	509	-	-	-	51.3	559	-	**2.06**	1.07	-	0.45	2.06
5		3-OL5	320	220	500	350	40	40	$4d_b20$	598	28	$8d_b12$	537	-	-	-	48.1	782	-	**2.71**	1.50	-	0.27	2.71
6		3-OL6	320	220	500	350	40	40	$4d_b20$	598	28	$16d_b12$	537	-	-	-	48.1	876	-	**2.71**	1.45	-	0.27	2.71
7		4-OL7	320	220	500	350	40	40	$4d_b25$	540	28	$12d_b12$	537	-	-	-	46.2	903	-	**2.98**	1.43	-	0.20	2.98
8		4-OL8	320	220	500	350	40	40	$4d_b25$	540	28	$24d_b12$	537	-	-	-	46.2	1088	-	**2.98**	1.41	-	0.20	2.98
9		1-DL1	320	220	500	350	40	40	$2d_b12$	537	30	$2d_b10$	509	165	$1d_b20$	598	56.8	245	-	1.77	1.39	**2.12**	1.00	2.12
10		1-DL2	320	220	500	350	40	40	$2d_b12$	537	30	$4d_b10$	509	165	$1d_b20$	598	56.8	283	-	1.77	1.39	**2.12**	1.00	2.12
11		2-DL3	320	220	500	350	40	40	$2d_b16$	599	32	$6d_b8$	521	56	$3d_b16$	599	56.4	472	-	**2.41**	1.22	0.81	0.86	2.41
12		2-DL4	320	220	500	350	40	40	$2d_b16$	599	32	$10d_b8$	521	56	$3d_b16$	599	56.4	555	-	**2.41**	1.02	0.81	0.86	2.41
13		3-DL5	320	220	500	350	40	40	$2d_b20$	598	28	$4d_b12$	537	60	$4d_b16$	599	49.6	628	-	**1.95**	1.61	0.62	0.53	1.95
14		3-DL6	320	220	500	350	40	40	$2d_b20$	598	28	$8d_b12$	537	60	$4d_b16$	599	49.6	728	-	**1.95**	1.16	0.62	0.53	1.95
15		4-DL7	320	220	500	350	40	40	$2d_b25$	540	28	$6d_b12$	537	65	$3d_b25$	540	52.0	868	-	**1.41**	1.11	0.52	0.37	1.41
16		4-DL8	320	220	500	350	40	40	$2d_b25$	540	28	$12d_b12$	537	65	$3d_b25$	540	52.0	995	-	**1.41**	1.00	0.52	0.37	1.41
17	4,7	DEB-1.1	200	125	300	250	45	45	$5d_b10$	567	35	$2d_b10 + 2d_b8$	587 *	-	-	-	41.1	193.6	-	1.27	**1.39**	-	0.52	1.39
18		DEB-1.2	200	125	300	250	45	45	$3d_b10$	567	35	$2d_b10 + 2d_b8$	587 *	-	-	-	39.3	132.7	145.8	**1.44**	1.40	-	0.58	1.44
19		DEB-1.3	200	125	300	250	45	45	$5d_b10$	567	36	$2d_b8$	619	-	-	-	39.9	121.1	133.0	1.28	**1.75**	-	1.00	1.75
20		DEB-1.4	200	125	300	250	45	45	$5d_b10$	567	36	$2d_b8$	619	-	-	-	40.4	183.0	170.4	1.28	**1.28**	-	0.49	1.28
21		DEB-1.5	200	125	300	250	45	45	$3d_b10$	567	36	$2d_b8$	619	-	-	-	40.8	125.3	-	1.43	**1.74**	-	1.00	1.74
22		DEB-1.6	200	125	300	250	42	42	$4d_b16$	550	32	$2d_b10$	544	-	-	-	31.1	309	251	**1.81**	1.20	-	0.16	1.81
23		DEB-1.7	200	125	300	250	44	44	$4d_b12$	546	34	$2d_b10$	544	-	-	-	30	194.4	188.8	**1.45**	1.21	-	0.27	1.45
24		DEB-1.8	200	125	300	250	44	44	$5d_b12$	546	34	$2d_b10$	544	-	-	-	32.2	195.3	199.1	**1.40**	1.23	-	0.23	1.40
25		DEB-1.9	200	125	300	250	44	44	$3d_b12$	546	34	$2d_b10$	544	-	-	-	31.9	141.7	145.5	**1.48**	1.23	-	0.38	1.48
26		DEB-2.1	200	125	300	250	45	45	$3d_b10$	567	36	$3d_b8$	619	55	$2d_b10$	567	40.2	194.9	199.6	1.22	**1.43**	0.88	0.84	1.43
27		DEB-2.2	200	125	300	250	44	44	$4d_b12$	546	34	$4d_b10$	544	56	$2d_b12 + 1d_b10$	545 *	33.3	322	330	**1.04**	0.87	0.41	0.29	1.04
28		DEB-2.3	200	125	300	250	44	44	$3d_b12$	546	32	$2d_b12$	546	56	$2d_b12$	546	33.3	241	-	1.12	**1.21**	0.57	0.58	1.21
29		DEB-2.4	200	125	300	250	45	45	$4d_b10$	548	33	$2d_b12$	552	55	$2d_b12 + 1d_b16$	548 *	36.9	312	309	**0.76**	1.07	0.38	0.60	0.76
30		DEB-2.5	200	125	300	250	46	46	$2d_b8$	554	36	$2d_b8$	554	54	$2d_b16 + 1d_b12$	546 *	37.1	265	295	1.30	**1.49**	0.33	1.00	1.49
31		DEB-2.6	200	125	300	250	42	42	$4d_b16$	544	34	$2d_b8$	554	58	$2d_b16 + 1d_b12$	546 *	38.3	328	-	1.16	**1.47**	0.33	1.00	1.47

*In cases of different bar diameters with different yield strengths, an effective yield strength is used that results in the correct yield force of the entire reinforcement.

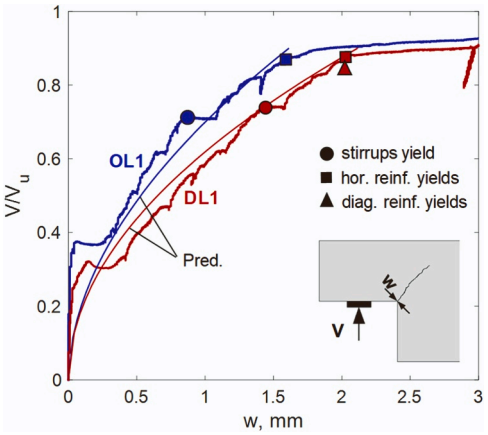

Fig. 3. Crack opening behavior of lightly-reinforced dapped-ends [11,12].

diagrams.

It can be seen from Fig. 3 that the two specimens exhibited similar responses, even though the dapped end with orthogonal reinforcement had better crack control (i.e., narrower cracks for the same load). There are several stages that can be distinguished in the response of the specimens. According to the measured curves, the re-entrant corner crack formed at $V/V_u \approx 0.35$. Following this initial stage, w increased gradually with increasing tension in the horizontal and vertical reinforcement across the crack, accompanied by increasing debonding of the reinforcement away from the crack. Using the strain gauges shown in Fig. 2, it was detected that the vertical reinforcement in both specimens yielded at $V/V_u \approx 0.75$. The failure of specimen OL1 was triggered by the yielding of the horizontal reinforcement, and that of DL1 by the simultaneous yielding of the horizontal and diagonal reinforcement. In both cases the yielding occurred at $V/V_u \approx 0.90$. From the point of view of strut-and-tie models, this failure corresponds to yielding of all ties near the re-entrant corner (Fig. 1b). Following this critical point, a plastic plateau with slight hardening was observed in the response of both specimens up to failure. It is important to note that, during most of the response of the lightly-reinforced dapped ands, there was a single dominant crack, namely the crack that propagated from the re-entrant corner (Fig. 4 top).

2.3. Behavior of heavily-reinforced dapped ends

The behavior of the lightly-reinforced dapped ends is contrasted to that of specimens OL8 and DL8 with heavy orthogonal and diagonal reinforcement, respectively. As in tests OL1 and DL1, the cracking initiated with the re-entrant corner crack. However, as shown in Fig. 4 (bottom), a series of parallel cracks developed subsequently, both above and below the corner crack. The failure occurred along a major shear crack, which extended from the inner edge of the loading plate to the top of the stirrups near the dapped end. Crushing of concrete was observed above the shear crack, consistent with crushing of the inclined strut in the dapped end (Fig. 1b). Even though strut crushing occurred, dapped ends OL8 and DL8 were already near failure due to yielding of most of the reinforcement in the vicinity of the re-entrant corner.

The behavior of the re-entrant corner crack of specimens OL8 and DL8 is shown in Fig. 5. Globally, the shape of the two (V/V_u)-w curves differed significantly from that observed in the lightly-reinforced specimens OL1 and DL1. Neglecting local variations, the dapped-ends with heavy reinforcement behaved in an approximately linear manner. In addition, in comparison to OL1 and DL1, the crack width trend is reversed: the specimen with diagonal reinforcement exhibited significantly better crack control than the specimen with orthogonal

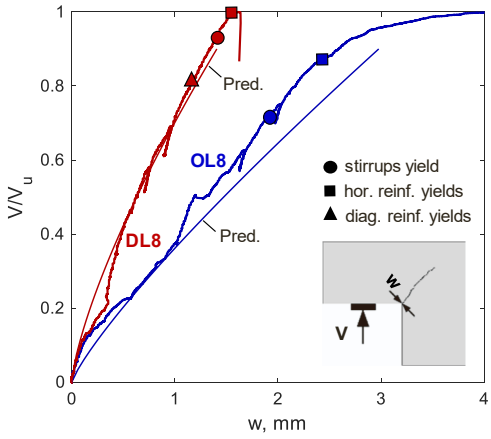

Fig. 5. Crack opening behavior of heavily-reinforced dapped-ends [11,12].

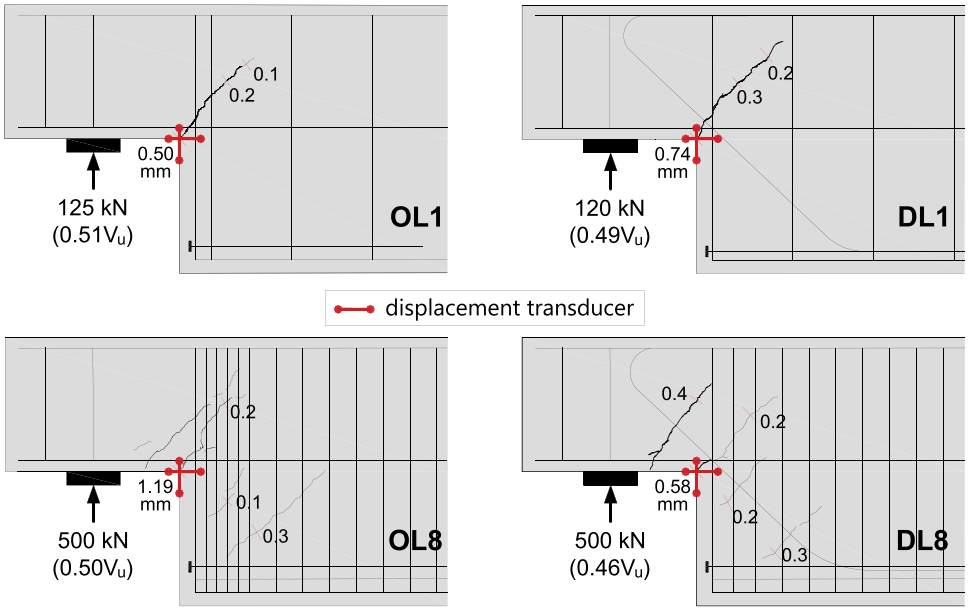

Fig. 4. Cracks in tests specimens at ~50% of peak load [11,12].

reinforcement. For the same load level $V/V_u \approx 0.5$, dapped end DL8 had crack widths that were approximately one-half of the widths measured in OL8.

Several stages can be distinguished along the measured curves in Fig. 5. First, it is noted that the corner crack began to open almost instantly with the application of the load. This is devoted to restrained shrinkage, which was larger in the heavily-reinforced specimens due to the stiffer reinforcement. Once the cracks formed, they opened in part due to the "release" of the shrinkage strains in the re-entrant corner.

Following this initial stage, a change of behavior occurred at $V/V_u \approx 0.22$. The response appears to "stiffen" due to the exhaustion of the shrinkage effect and the formation of secondary cracks. The secondary cracks provide crack control such that the re-entrant corner crack opens in a slower manner with increasing load. Using strain gauge measurements in the corner crack (Fig. 2), it was detected that the vertical reinforcement in specimen OL8 yielded first at $V/V_u \approx 0.71$, followed by the horizontal reinforcement at $V/V_u \approx 0.86$. In specimen DL8, the yielding of the diagonal, vertical and horizontal reinforcement occurred within a small load range. The diagonal bars yielded at $V/V_u \approx 0.82$, the stirrups at $V/V_u \approx 0.83$, and the horizontal bars were on the verge of yielding at failure. Dapped end DL8 did not exhibit a plastic plateau because concrete (strut) crushing occurred almost simultaneously with the yielding.

Fig. 6 summarizes the measured responses of specimens OL1, DL1, OL8 and DL8. In this plot the applied shear is not normalized to illustrate the difference in cracking load, stiffness, and ultimate capacity between the dapped ends. As the total amount of dapped end reinforcement was increased approximately 6 times from specimens OL1/DL1 to OL8/DL8, the ultimate capacity increased approximately 4 times. Globally, due to the large amount of reinforcement in specimens OL8/DL8, their response up to yielding was significantly stiffer than that of the two specimens with light reinforcement (the cracks opened slower with the applied load). However, this trend is reversed in the range of initial loading as highlighted in the figure. As mentioned earlier, this initial behavior is explained with restrained shrinkage, which is higher in dapped ends with larger amounts of reinforcement. Owing to the restraint of the shrinkage imposed by the steel bars, tension develops in the concrete prior to loading, resulting in premature cracking and softer initial response as compared to dapped ends with light reinforcement.

2.4. Key experimental observations

Based on the tests of lightly- and heavily- reinforced dapped-ends with orthogonal and diagonal reinforcement, the following important observations are made:

- Restrained shrinkage causes premature cracking and fast early opening of the re-entrant corner crack in dapped ends with heavy reinforcement.
- At higher loads, secondary cracks in such specimens help to control the opening of the re-entrant corner crack.
- In well-designed dapped-end connections with adequate anchorage of the reinforcement, the strength of the connection is governed mainly by yielding of the reinforcement in the re-entrant corner crack.

In the following, these observations are reflected in the derivation of a mechanical model for the (V/V_u)-w response of dapped-end connections.

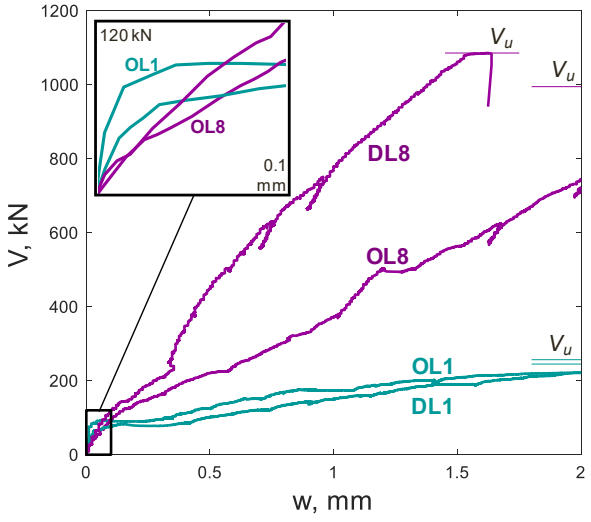

Fig. 6. Initial and global response of specimens with light (OL1 and DL1) and heavy (OL8 and DL8) reinforcement [11,12].

3. Yield point of dapped-end connections

3.1. Sequence of yielding and V/V_u at yielding of the connection

A starting point in the development of the model is the yield point of dapped-end connections. As it was observed earlier, this point occurs at $V/V_u \approx 0.80$–1.00, and is governed by the reinforcement which yields last. Therefore, it is first of interest to determine the sequence of yielding of the horizontal, vertical, and diagonal reinforcement. To this end, it is instructive to consider the kinematics of the crack at the re-entrant corner of dapped-end connections.

As mentioned earlier, in the 16 tests performed by Rajapakse at al. [11,12] with a wide range of variables, it was observed that the horizontal and vertical crack displacements had similar values. The difference between w_h and w_v was negligible in the specimens with light reinforcement, as well as in the initial response of dapped ends with medium and heavy reinforcement. Some differences were observed after the formation of secondary cracks, but without a clear trend with respect to the tests variables [11,12]. The differences are therefore devoted mainly to the complex nature of secondary cracks, variability in the inclination of the corner crack, and local debonding of the reinforcement.

These observations are compatible with the global kinematics of dapped-end connections illustrated in Fig. 7 [11,17]. In this idealized kinematics, the re-entrant corner crack is straight and inclined at ~45°. The crack divides the connection into two blocks, which rotate with respect to each other about the tip of the crack. As the blocks rotate, the crack widens and compressive strains/stresses develop above the tip of the crack. Crack displacements w_h and w_v are necessarily equal in this model. Therefore, taking into account the test measurements and global kinematics, it will be assumed that $w_h \approx w_v$.

This assumption allows to evaluate the width of the re-entrant corner crack w based on the yielding of each reinforcement. If the horizontal reinforcement yields at $w_h = w_{hy}$, the corresponding crack width is:

$$w_{y,1} = \frac{w_{hy}}{\sin 45^\circ} \tag{1}$$

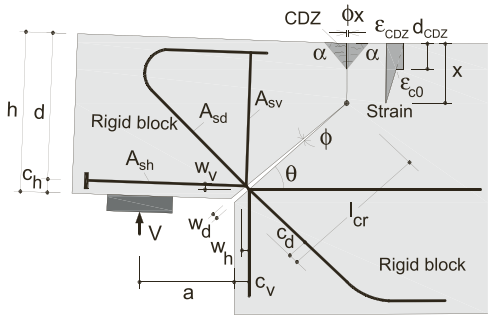

Fig. 7. Idealized kinematics associated with corner cracks in dapped-end connections [11,17].

If the vertical reinforcement yields at $w_v=w_{vy}$, the crack width is:

$$w_{y,2} = \frac{w_{vy}}{\cos 45^\circ} \quad (2)$$

And if the diagonal reinforcement yields at $w_d=w_{dy}$, the crack width is:

$$w_{y,3} \approx w_{dy} \quad (3)$$

The minimum of crack widths $w_{y,1}$, $w_{y,2}$ and $w_{y,3}$ will determine which reinforcement will yield first, and the maximum will determine which yields last. Therefore, to evaluate the yield crack width of the dapped-end connection, it is necessary to evaluate the maximum value obtained from the horizontal, vertical, and diagonal reinforcement. As for V/V_u at the yielding of the connection, an average value of 0.9 will be assumed. This value takes into account that certain strain hardening occurs after yielding.

3.2. Yield crack width of dapped-end connections

3.2.1. Dapped ends with orthogonal reinforcement

In dapped-ends with orthogonal reinforcement layout, the yield crack displacement w_y is typically governed by the horizontal reinforcement. This is because the horizontal bars usually have bigger diameters than the vertical reinforcement (stirrups). Therefore, in the absence of diagonal reinforcement, the yield crack displacement is calculated from Eq. 4.

$$w_y = w_{y,1} = \sqrt{2} w_{hy} \quad (4)$$

The derivation of the horizontal yield opening w_{hy} is based on the idealized strain diagram in Fig. 8. The diagram shows how the strains in the main horizontal reinforcement ε_s vary away from the corner crack at two load levels. The first load level corresponds to the stage when a major secondary crack is about to form in the dapped end. As observed in the tests, this crack typically extends from the inner edge of the loading plate (shear crack) and is approximately parallel to the corner crack. The maximum tension force in the reinforcement at this stage is denoted as T_{cr}. Because the concrete in the dapped end and full-depth section is still uncracked, the strains in the reinforcement decrease linearly away from the corner crack. The linear decrease corresponds to a constant bond stress τ_b along the reinforcement [18]. The bond stress is assumed zero only in the immediate vicinity of the crack (see the zone of constant ε_s), where local debonding occurs due to cone-shape splitting of concrete. The length of debonding l_0 is estimated at two bar diameters [19] plus the concrete cover ($2d_{bh}+c_1$).

The second load level in Fig. 8 corresponds to the yielding of the horizontal reinforcement in the corner crack ($\varepsilon_{s,max}= \varepsilon_y$). The maximum tension in the reinforcement at this stage is denoted as T_y. In the full-depth section, the secondary cracks are relatively narrow and do not fully cross the horizontal reinforcement. Therefore, the strain profile in this region remains linear, but extends farther away from the corner crack. In contrast, in the dapped-end region, the profile is significantly modified by the major shear crack. In this region, a portion of the strain diagram will contribute to the opening of the corner crack, and the rest to the opening of the shear crack. The strains that contribute to the corner crack are highlighted in blue in Fig. 8. In the range $T_{cr}<T \leq T_y$, the strains due to force increment (T-T_{cr}) are assumed to extend at distance $a_{cl}/2$ from the corner crack. Length a_{cl} is the distance between the two major cracks, which coincides with the distance from the re-entrant corner of the connection to the inner edge of the loading plate.

Using the above assumptions, w_{hy} is obtained by integrating the

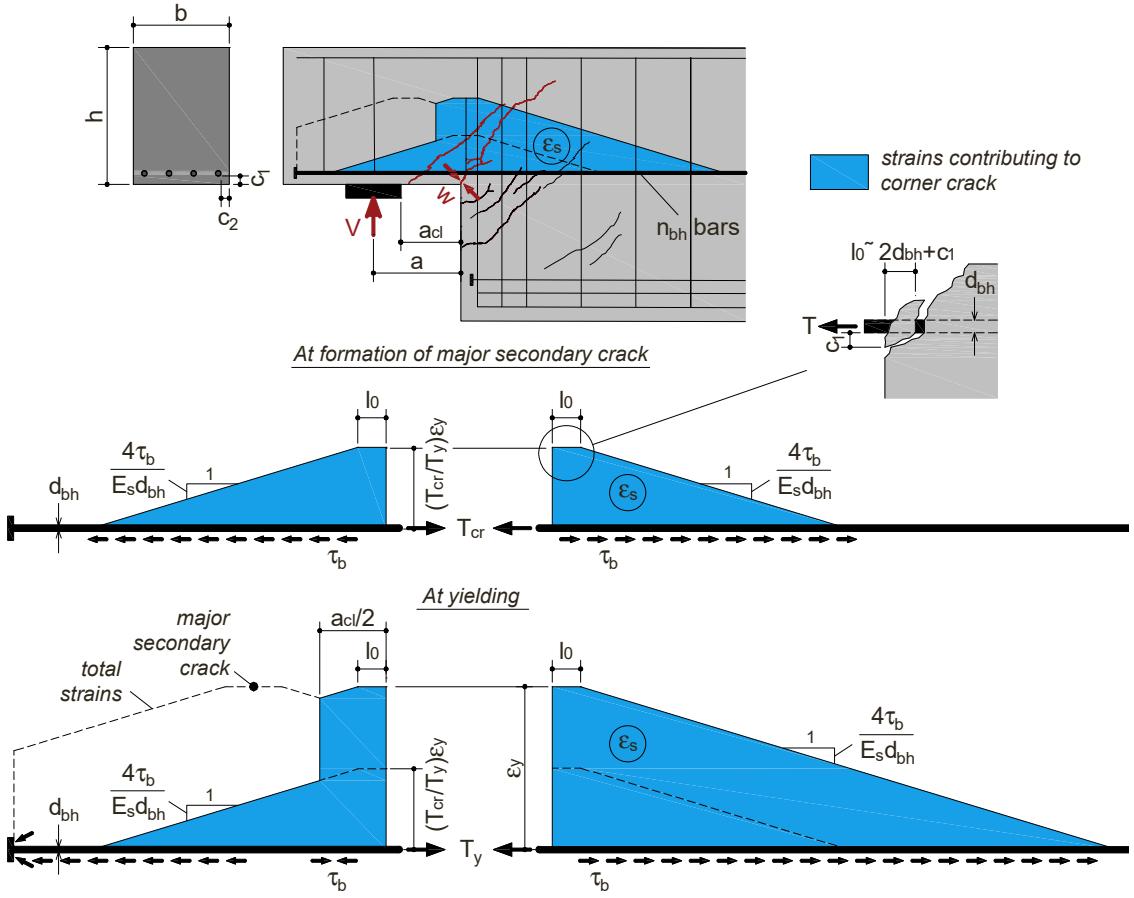

Fig. 8. Idealized strain profile along horizontal reinforcement at yielding.

highlighted strain profile at $T = T_y$:

$$w_{hy} = \frac{E_s d_{bh}(1 + {k_{cr}}^2){\varepsilon_y}^2}{8\tau_b} + (2d_{bh} + c_1)(1 + k_{cr})\varepsilon_y + 0.5a_{cl}(1 - k_{cr})\varepsilon_y \quad (5)$$

where E_s is the modulus of elasticity of the steel, d_{bh} is the diameter of the horizontal bars, $\varepsilon_y = f_y/E_s$ is the yield strain of the steel, and f_y is the yield stress. Quantity k_{cr} is the ratio of forces T_{cr} and T_y:

$$k_{cr} = \min\left(\frac{T_{cr}}{T_y}, 1.0\right) \quad (6)$$

$$T_{cr} \approx 0.5hb.f_{ct} \quad (7)$$

$$T_y = A_{sh}.f_y \quad (8)$$

where $f_{ct} \approx 0.33\sqrt{f_c}$ (MPa) is the tensile strength of the concrete, h is the depth of the dapped end, b is the width of the dapped end, and A_{sh} is the total area of main horizontal reinforcement in the dapped end. The proposed expression for T_{cr} is a simple approximation of a complex process of secondary cracking in dapped ends. Nevertheless, the result of Eq. 5 is not very sensitive to the k_{cr} ratio, and therefore this simplification is justified. If $T_{cr} \geq T_y$, no cracking is expected in the dapped end, and k_{cr} is 1.0.

Finally, the bond strength τ_b is evaluated as

$$\tau_b = \min\left(2, \frac{c + d_{bh}/2}{1.664d_{bh}}\right)f_{ct} \quad (9)$$

where c (mm) is the minimum concrete cover c_1 or c_2 of the horizontal reinforcement – see Fig. 8. In this expression, $2f_{ct}$ is the bond strength in the absence of significant splitting of the concrete around the bars [20]. Splitting may occur in dapped ends with large bars and/or small concrete cover, causing reduced bond strength. This effect is taken into with the second term in the brackets as proposed by Tepfers [21].

In cases where the vertical reinforcement has large diameters, w_{vy} can also be calculated from Eq. 5. In such cases d_{bh} and A_{sh} are replaced by d_{bv} and A_{sv}, and $c \equiv c_1$ becomes the minimum concrete cover of the vertical reinforcement. The crack width at yielding w_y is then obtained as the maximum of $w_{y,1}$ and $w_{y,2}$ (Eqs. 1 and 2).

It is important to note that Fig. 8 explains the difference between re-entrant corner cracks in dapped ends and flexural cracks in beams. In beams, multiple flexural cracks typically form at approximately the same time at low load levels. For this reason, crack widths in design codes are typically estimated as the average strain in the reinforcement times the spacing of the cracks. In dapped ends with light to moderate reinforcement, this will result in unrealistically small crack widths of approximately $a_{cl} \times \varepsilon_y$. This estimate does not reflect the behavior of dapped ends where the secondary cracks form significantly later than the corner crack (or may not form at all). Because of this delayed cracking, significant crack opening occurs before the development of secondary cracks as evident from the strain diagram at $T = T_{cr}$ in Fig. 8. It is this initial opening that causes wide cracks in dapped-ends. In Eq. 5, this effect is captured by factor k_{cr}. When the reinforcement is light and k_{cr} is 1, there is a single crack, and the crack width is entirely determined by the top strain diagram at $T = T_{cr}$. If the reinforcement is heavy and k_{cr} tends to zero, the secondary cracks form soon after the corner crack, and the crack width according to Eq. 5 has a minimum.

Note also that $(1/k_{cr})$ has a meaning of mechanical reinforcement ratio, which can be linked to restrained shrinkage. When $(1/k_{cr})$ is 1, the mechanical reinforcement ratio has a minimum, and the retrained shrinkage also has minimum. Inversely, when $(1/k_{cr})$ is larger than 1, the mechanical reinforcement ratio increases, and the restrained shrinkage increases as well. The restrained shrinkage is neglected in Eq. 5 because its effect at yielding is relatively small. However, at low load levels, the shrinkage effect will be taken into account indirectly via the k_{cr} ratio.

3.2.2. Dapped ends with diagonal reinforcement

In dapped ends with diagonal reinforcement, the yield crack displacement w_y is typically governed either by the horizontal or by the diagonal reinforcement:

$$w_y = \max(w_{y,1}, w_{y,3}) = \max(\sqrt{2}w_{hy}, w_{dy}) \quad (10)$$

Crack opening w_{hy} is derived as before based on Fig. 8, except for one difference associated with the diagonal reinforcement. In the presence of diagonal bars, there is a modification of the cracks in the full-depth section. Because the diagonal reinforcement is symmetrical with respect to the re-entrant corner of the connection, it forces major secondary cracking on both sides of the corner crack (see specimen DL8 in Fig. 4). In other words, the corner crack is not controlled mainly by the cracking in the dapped end (shear crack), but also by the cracking in the full-depth section. To take this into account, the strain profile in the dapped end is also applied to the full-depth section (symmetrical strain profile):

$$w_{hy} = \frac{E_s d_{bh}(k_{cr}\varepsilon_y)^2}{4\tau_b} + 2(2d_{bh} + c_1)k_{cr}\varepsilon_y + a_{cl}(1 - k_{cr})\varepsilon_y \quad (11)$$

where the quantities in this equation remain as defined before. This expression is valid if there is a sufficient amount of diagonal reinforcement to control the cracks along the horizontal reinforcement in the full-depth section. In cases of relatively small diagonal reinforcement, it is necessary to transition between Eq. 5 and Eq. 11. If there is no diagonal reinforcement (A_{sd}=0), Eq. 5 applies, and if $(A_{sd}\sqrt{2})/A_{sh} \geq 1$, Eq. 11 applies. A linear interpolation between the two values of w_{hy} can be used when the ratio $(A_{sd}\sqrt{2})/A_{sh}$ has a value between 0 and 1.

To evaluate the crack width corresponding to yielding of the diagonal reinforcement, a symmetrical strain profile is used as in Eq. 11:

$$w_{dy} = \frac{E_s d_{bd}(k_{cr}\varepsilon_y)^2}{4\tau_b} + 4d_{bd}k_{cr}\varepsilon_y + 0.5\sqrt{2}a_{cl}(1 - k_{cr})\varepsilon_y \quad (12)$$

where d_{bd} is the diameter of the diagonal bars. Multiplier $\sqrt{2}$ is introduced to take into account that the crack spacing in the direction of the diagonal reinforcement is approximately $a_{cl} \times \sin 45^\circ$, where a_{cl} is the horizontal spacing (Fig. 8). The cracking tensile force T_{cr} is estimated from Eq. 7 as before, and T_y is equal to $A_{sd}.f_y$. The bond strength is calculated from Eq. 9, where c is equal to the side concrete cover c_2 of the diagonal bars ($c \equiv c_2$). The bottom cover c_1 is not relevant for diagonal bars, as they are embedded deeply in the dapped end and in the full-depth section.

In cases where the vertical reinforcement has large diameters, w_{vy} can be calculated from Eqs. 5 and 11. In such cases d_{bh} and A_{sh} are replaced by d_{bv} and A_{sv}, and $c \equiv c_1$ becomes the minimum concrete cover of the vertical reinforcement. The crack width at yielding w_y is then obtained as the maximum of $w_{y,1}$, $w_{y,2}$, and $w_{y,3}$ (Eqs. 1–3).

4. Modeling the complete *v-w* response

4.1. Shape of V-w response

The formulation presented so far focused on the yield point of dapped-end connections. The crack width at yielding w_y is evaluated from Eq. 4 and Eq. 10 for connections with orthogonal and diagonal reinforcement, respectively. The yield force V_y is estimated at 90% of the ultimate capacity V_u. Having defined the yield point, the next step is to model the shape of the *V-w* response from zero load up to yielding.

Fig. 9 illustrates the complete response of the 16 specimens by Rajapakse et al. [11,12]. On the horizontal axis is the crack width normalized by the measured width at yielding w_y, and on the vertical axis is the shear force normalized by the yield force V_y. Therefore, the yield point in these plots has unit x and y coordinates. The shading of the curves reflects the amount of reinforcement in the test specimens. The

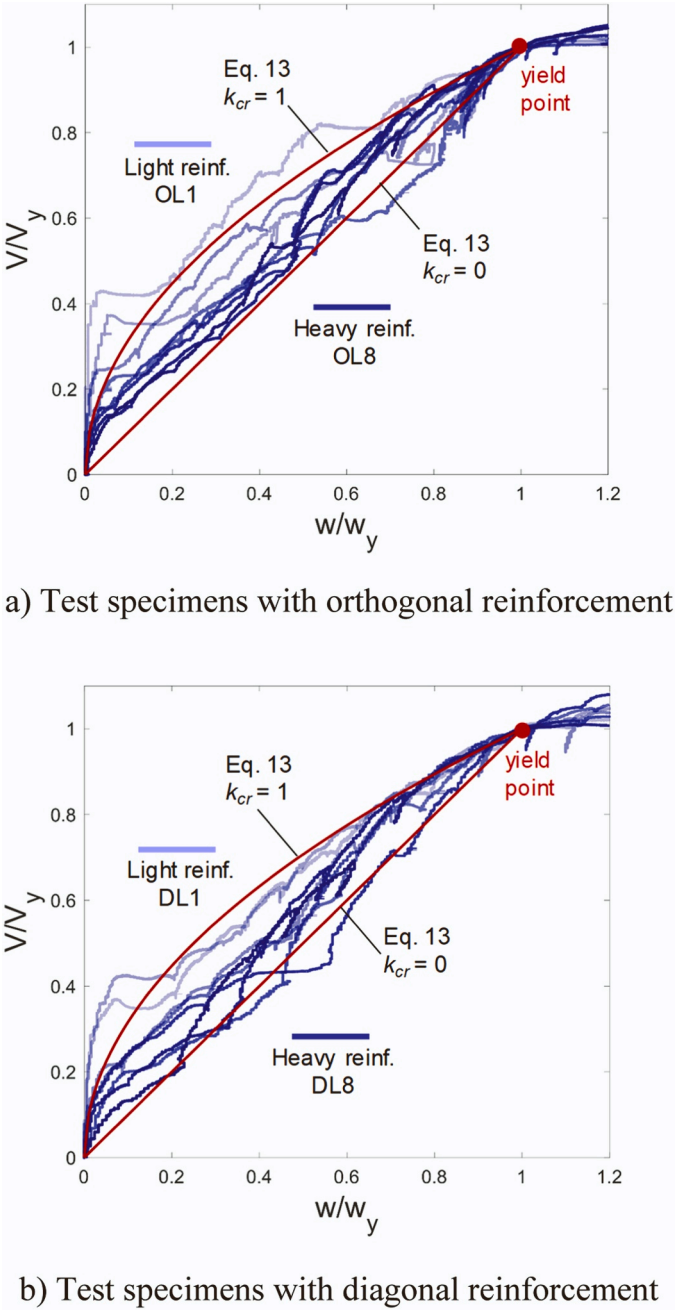

Fig. 9. Normalized shear force versus crack width response.

lightest shade corresponds to the specimens with the lightest reinforcement (OL1 and DL1), and the darkest shade to those with the heaviest reinforcement (OL8 and DL8).

As evident from Fig. 9, dapped ends with orthogonal and diagonal reinforcement exhibited similar normalized responses. In both cases, the measured curves fall almost exclusively between two idealized responses, shown with red curves. The top idealized response corresponds to an exponential function, and the bottom normalized response corresponds to a linear function. Additionally, there is a clear trend with respect to the amount of reinforcement. The response of the specimens with the lightest reinforcement is the closest to the exponential function, and the response of the specimens with the heaviest reinforcement is the closest to the linear function.

Based on these observations, the following expression for the complete normalized response of dapped-end connections is proposed:

$$w = w_y \left(\frac{V}{0.9V_u} \right)^{1+k_{cr}} \tag{13}$$

where w_y is calculated as discussed earlier, and k_{cr} is obtained on the basis of the reinforcement that governs the w_y prediction (typically the horizontal or diagonal reinforcement). The shear force at yield V_y is estimated at $0.9V_u$, where V_u is the ultimate capacity of the dapped-end connection. Eq. 13 provides the width of the re-entrant corner crack for a given ratio between the applied shear force V and the ultimate capacity V_u of the connection. This makes the equation very convenient for rapid checks of crack widths under service loads. If the V/V_u ratio at service conditions is known (e.g. ~0.5–0.6), this expression can be used directly to verify whether the crack width is within the limits specified in design codes.

Eq. 13 has a clear physical meaning. The effect of the reinforcement amount on the shape of the response is reflected by the factor k_{cr}. In dapped ends with light reinforcement, there is a single crack at the re-entrant corner and k_{cr} is equal to 1.0. In this case the idealized response is represented by the exponential curve in Fig. 9. By shape, this response resembles the pullout behavior of bars embedded in uncracked concrete [18]. Indeed, the response of dapped ends with light reinforcement is governed by the pullout behavior of the bars on both sides of the re-entrant corner crack. Shrinkage is not a major factor in such dapped ends, because the small amount of reinforcement does not provide a significant restraint on the shrinkage.

In dapped ends with heavy reinforcement, there are multiple cracks, and k_{cr} tends to 0. That is, the mechanical reinforcement ratio ($1/k_{cr}$) is large. In such cases, the shrinkage strains are restrained and cause increased widths of the corner crack at low loads (Fig. 6). As the load increases, this trend is countered by the secondary cracks which provide crack control. As a result, the global trend from zero load to yielding is close to linear. At the yielding of the reinforcement, the effect of restrained shrinkage is relatively small (the cracks are wide), and for this reason it was neglected in Eq. 5 and Eqs. 11–12 for w_{hy} and w_{dy}.

4.2. Ultimate capacity Vu

As mentioned earlier, Eq. 13 is convenient from a practical point of view, because it expresses the crack width as a function of the relative load level V/V_u. For rapid serviceability calculations, this ratio can be assumed equal to the ratio of the shear due to service loads and the shear due to design loads. For more refined calculations, it may also be of interest to calculate the ultimate capacity V_u, as in some cases it may be significantly larger than the shear due to design loads. This can allow to lower the calculated crack width in order to comply with crack width limits.

There are several different approaches to calculate V_u with variable levels of complexity and accuracy. Strut-and-tie models as the ones shown in Fig. 1b are relatively simple to use, and typically provide conservative perditions [1–5]. Refined calculations can be performed with more complex stress field approaches, which can significantly improve the accuracy [7]. To balance simplicity and accuracy, Rajapakse et al. [17] have proposed a kinematics-based model for the strength of dapped-end connections failing along a re-entrant corner crack (flexural failure). This model is based on the kinematics presented in Fig. 7, and also includes equilibrium conditions and stress-strain relationships for the materials. Any of these approaches can be used with the crack width model proposed in this study. The more conservative is the model for V_u, the more conservative will be the calculation of the crack width under service loads.

5. Validation with test results

5.1. Yield crack width

The proposed model for crack widths is first validated with the tests performed by Rajapakse et al. [11,12]. To generate the normalized plots in Fig. 9, the crack width at yielding w_y of each test specimen was obtained from the measured *V-w* responses. These experimental values are plotted in Fig. 10, separately for the specimens with orthogonal and diagonal reinforcement. The figure also shows the predictions of Eq. 4 and Eq. 10, respectively. On the horizontal axis is the total area of horizontal, vertical and diagonal reinforcement.

It can be seen from the test results that, on average, the yield crack widths of dapped ends with orthogonal reinforcement are larger than those of the specimens with diagonal reinforcement. The values for specimens OL1 to OL8 varied between ~1.5 mm and ~3 mm, while those of specimens DL1 to DL8 between ~1.5 mm and ~2 mm. It is interesting to note that the global trends in the two sets of data are reversed. The increase of reinforcement (and bar diameters) in specimens OL1 to OL8 resulted in increasing w_y, while the opposite is observed for the diagonally-reinforced specimens DL1 to DL8. Overall, these trends are captured by the proposed model, even though some significant deviations are observed for individual specimens. The deviations are in part due to the natural scatter associated with the complex phenomena of restrained shrinkage, cracking, and bond in dapped-end connections. The scatter appears to be more significant in the specimens with orthogonal reinforcement.

The proposed model can be used to explain the opposite trends observed in the OL and DL tests in Fig. 10. There are three opposing effects on crack widths according to Eq. 5 and Eqs. 11–12. As the bar diameters increase, the strains in the reinforcement penetrate deeper in the concrete on both sides of the corner crack, and therefore w_y increases. Also, as the bar diameters increase, the bond strength decreases due to local splitting of the concrete (Eq. 9), leading to further strain penetration. At the same time, as the amount of reinforcement increases, the crack control increases as well (k_{cr} tends to 0), and therefore w_y decreases. This latter effect governs in dapped ends with diagonal reinforcement, where crack control occurs on both sides of the re-entrant corner crack (i.e. in the dapped end and full-depth section). In contrast, in dapped-end connections with orthogonal reinforcement, the crack control is mainly on one side of the corner crack (i.e., in the dapped end), and it is not able to counter the effect of increasing bar diameters.

5.2. Complete V-w response

The predictions of the proposed model for the complete response of specimens OL1/DL1 and OL8/DL8 are shown respectively in Fig. 3 and Fig. 5. As discussed earlier, the main difference between the pairs of specimens in each plot is the reinforcement layout: orthogonal versus diagonal. Specimens OL1/DL1 were lightly reinforced and OL8/DL8 had ~4 times larger reinforcement. It can be seen that the model captures well the complete response of the four specimens, both in terms of overall shape and values. The model also predicts correctly that OL1 had slightly narrower cracks than OL8, while DL1 had significantly wider cracks than DL8.

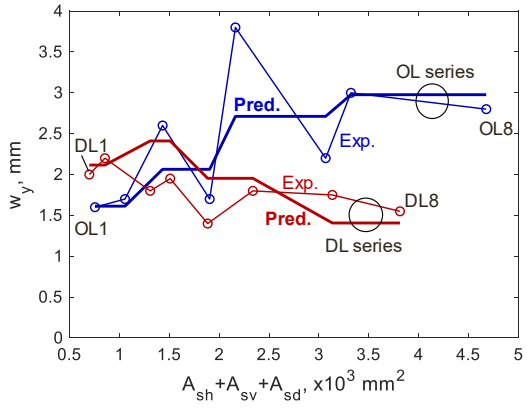

Fig. 10. Measured and predicted crack width at yielding of dapped ends with orthogonal (OL) and diagonal (DL) reinforcement layout.

Similar observations can be made for all 16 specimens tested by Rajapakse et al. [11,12] as shown in Fig. 11a. The top 4 plots correspond to specimens with orthogonal reinforcement, while the bottom 4 plots to specimens with diagonal reinforcement. Each plot compares two specimens with the same horizontal (and diagonal) reinforcement, but different vertical reinforcement near the dapped end. The darker curves correspond to two times larger vertical reinforcement than the lighter curves. It can be seen that, in most cases, the amount of vertical reinforcement had a negligible effect on the crack width as predicted by the model. Exceptions are specimens OL5/6 and DL5/6, where the difference is significant but without a clear trend: OL5 had wider cracks than OL6, while DL5 had narrower cracks than DL6. This indicates that the difference is mainly due to natural scatter in crack widths. It can be seen that in cases of large scatter, the proposed model tends to capture the average response.

Similar analyses were performed for 26 tests performed by Mata Falcón [4,7] with orthogonal and diagonal reinforcement. The properties of the specimens are summarized in Table 1 and the V/V_u-*w* curves are presented in Fig. 11b. With the exception of specimens DEB1.1, DEB1.5, DEB2.3 and DEB2.6, all plots show the results from two nominally identical specimens (test T1 and test T2). It can be seen that in some cases the scatter between the responses of identical dapped ends can be significant, confirming the observation made on the basis of specimens OL5/6 and DL5/6. With a few exceptions, the proposed model captures well the average response of the pairs of specimens.

Fig. 12 illustrates how the proposed model for crack widths can be used in combination with an appropriate model for the ultimate capacity V_u of dapped-end connections. Specimens OL1 and OL2 differed only in the amount of vertical reinforcement, and therefore had the same predicted response in terms of normalized shear force V/V_u versus crack width *w* (Fig. 11a). In Fig. 12, the V/V_u axis is multiplied by the ultimate capacity of the two dapped ends obtained with the kinematics-based model [17]. The model predicts that as the vertical reinforcement is increased from 8ϕ10 mm bars to 12ϕ10 mm bars, the ultimate capacity increases from 451 kN to 516 kN [11,12]. This results in two distinct *V-w* responses, which agree well with the measured response of specimens OL1 and OL2. The measured ultimate capacity of the two specimens was respectively 471 kN and 555 kN. The same approach is followed for specimens OL3 and OL4 in Fig. 12, resulting in similarly adequate predictions of *V-w* response.

It is important to note that the comparisons performed in Figs. 11 and 12 require straightforward input and simple "hand" calculations. At the same time, the proposed equations are built on mechanics and reflect the governing phenomena in dapped-end connections. In this manner, they can be used for rapid calculations, as well as to develop understanding of the crack-opening behavior of dapped ends. As the equations contain a small number of input properties (i.e., basic geometrical and material properties), they can be used by engineers to examine the effect of key parameters influencing crack widths in order to achieve adequate designs.

6. Effect of design parameters

To illustrate the effect of key parameters on the width of the corner crack, the proposed model is applied to five sample dapped ends. The connections have the same dimensions as those examined in Fig. 12, but differ in terms of reinforcement as summarized in Fig. 13. It is assumed

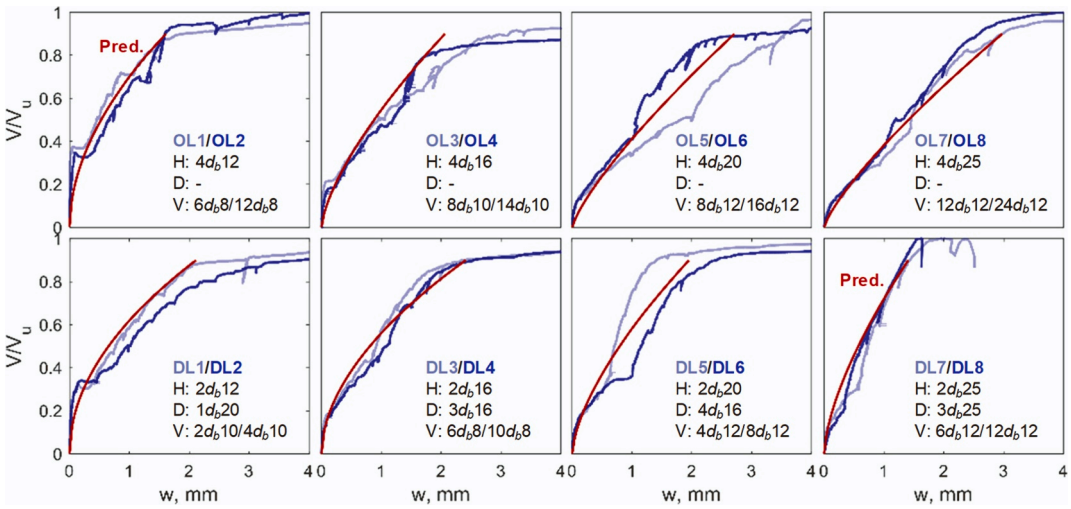

a) Tests by Rajapakse et al. [11][12]

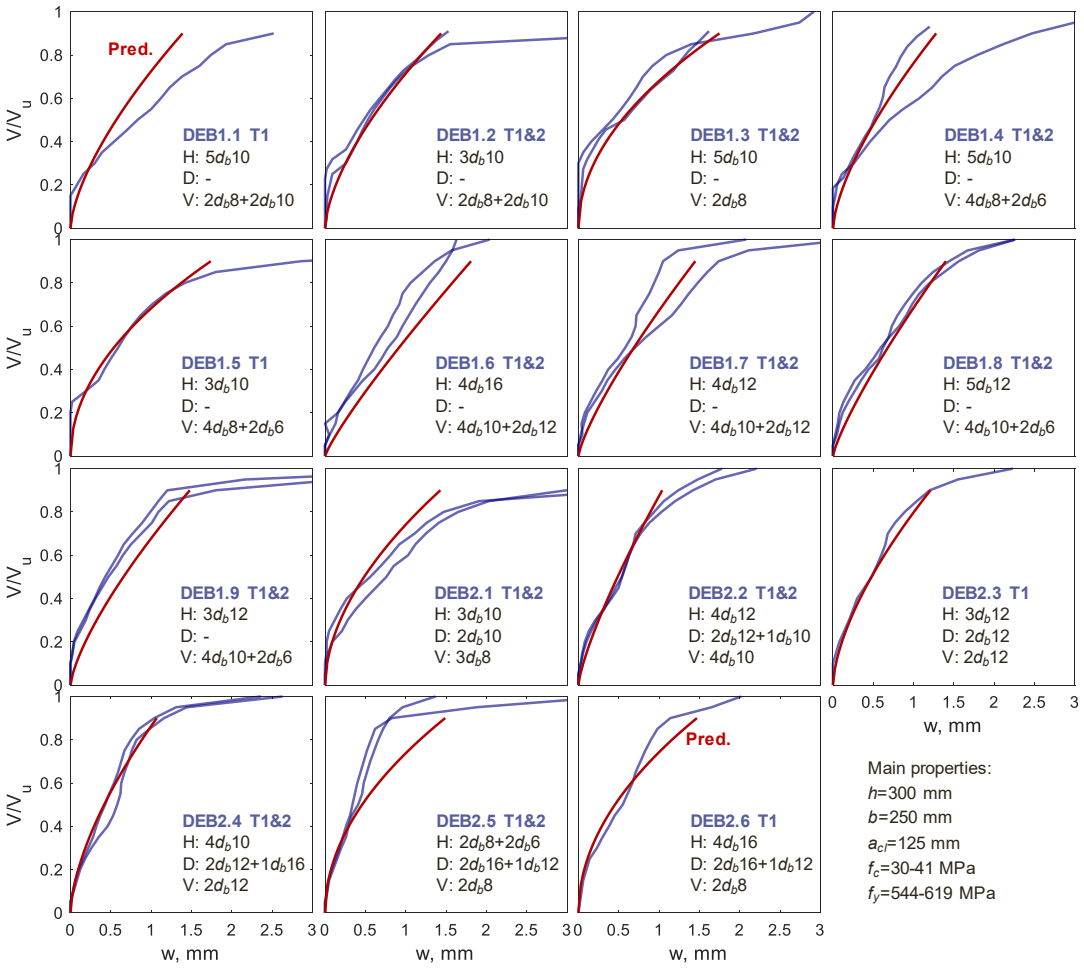

b) Tests by Mata Falcón [4][7]

Fig. 11. Measured and predicted complete response with normalized shear.

that the serviceability load level is V/V_u= 0.5, and that the limit on the crack width is w_{max}= 0.4 mm. Fig. 13a shows two designs with medium amounts of reinforcement, while Fig. 13b shows three designs with heavy reinforcement. The reinforcement within each plot is varied in a manner to maintain an approximately constant ultimate capacity V_u. Note that the distinction between "medium" and "heavy" reinforcement is not rigorous, and is made mainly for the sake of the discussion. The proposed model offers continuous equations, and therefore this distinction is not required for the purpose of design. Nevertheless, it is instructive to calculate the flexural reinforcement ratios of the dapped ends (horizontal reinforcement), and to compare them to the minimum and maximum ratios for flexure. The ratios of dapped ends A (Fig. 13a)

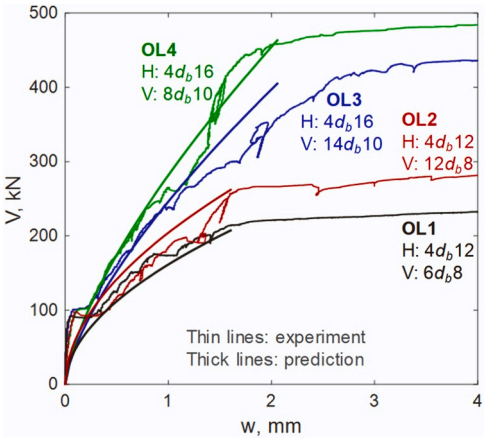

Fig. 12. Measured and predicted shear force versus crack width response.

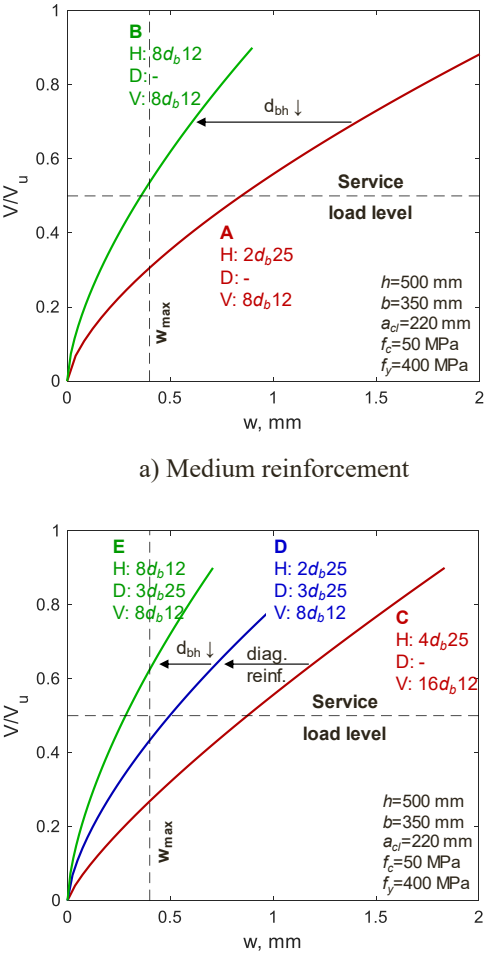

Fig. 13. Effect of crack control parameters.

and C (Fig. 13b) are 0.62% and 1.25%, respectively, while the minimum and maximum ratios according to Eurocode 2 [5] are 0.18% and 1.95% (concrete class C40/50 and reinforcement with f_y=500 MPa).

The reference dapped end in Fig. 13a is design A with 2d_b25 mm horizontal reinforcement and no diagonal bars. For this case, the crack width at service load is predicted at ~0.8 mm, and therefore the design is not compliant. To improve the design, in case B the horizontal reinforcement is replaced by 8d_b12 mm (2 layers of 4 bars). It can be seen that smaller bar diameters result in a significant reduction of crack width (w=0.36 mm), and in this way design B satisfies the crack width limit.

In heavily-loaded dapped ends it may not be practical (or even possible) to reduce the bar diameters without adding diagonal reinforcement. The reference dapped end in Fig. 13b is design C with 4d_b25 mm horizontal bars and no diagonal bars. Its crack width is predicted at ~0.8 mm, exceeding significantly w_{max}. As a first measure, some of the orthogonal reinforcement is replaced with diagonal bars in design D, such that the two reinforcement layouts carry approximately the same shear (A_{sd}≈$A_{sh}/\sqrt{2}$). This results in 2d_b25 mm horizontal bars and 3d_b25 mm diagonal bars, reducing the crack width to 0.5 mm. In the last step, a compliant design E is achieved by modifying the horizontal reinforcement of case D. Design E has 8d_b12 mm horizontal bars and 3d_b25 mm diagonal bars, resulting in a crack width of only 0.34 mm.

These examples illustrate that, in dapped ends with light to moderate reinforcement, the control of the re-entrant corner crack is feasible with orthogonal reinforcement only. In such cases the choice of bar diameters has a significant impact on the crack width at service conditions. On the other hand, in heavily-loaded dapped ends, it is also necessary to provide diagonal reinforcement that carries a significant portion of the applied shear (e.g. ~50%). Such reinforcement ensures distributed cracking both in the dapped-end and full-depth section, and in this way reduces the width of the dominant corner crack.

7. Summary and conclusions

In this study, detailed experimental data was used to provide an in-depth understanding of the opening of re-entrant corner cracks in dapped-end connections. The experimental observations were used to develop a rational model for rapid assessment of crack widths from zero load up to yielding of the connection. The model was validated with 42 tests of dapped ends with a broad range of properties, including orthogonal and diagonal reinforcement layouts. The main findings of the study are the following:

1) Restrained shrinkage effects cause premature cracking and fast early opening of the re-entrant corner crack in dapped-end connections with heavy reinforcement. At higher loads, secondary cracks in such connections help to control the opening of the crack.
2) In well-designed dapped-end connections with adequate anchorage of the reinforcement, the strength of the connection is typically governed by yielding of the reinforcement in the re-entrant corner crack. The width of the re-entrant corner crack at yielding can be evaluated in a rational manner, by modeling the reinforcement strains in the vicinity of the re-entrant corner as affected by the dominant corner crack and secondary cracking.
3) With a predicted yield point, it was shown that the shape of the shear force versus crack width response varies gradually between two limit cases consistent with findings 1) and 2). A simple equation with a clear physical meaning was derived to capture this transition depending on the amount of reinforcement.
4) The validation studies showed that the proposed model predicts well the complete crack-opening response from zero load up to yielding of the connection. The comparisons with tests showed also that the response is governed mainly by the reinforcement with the largest bar diameters (horizontal, vertical or diagonal), and this is captured by the model.
5) The main properties affecting the width of the cracks are the amount and detailing of the dapped-end reinforcement. It was shown that the proposed model captures well the effect of these variables, and therefore can be used to design for crack control at service conditions. As the model is applicable up to the yielding of the connection, it has the potential to also be extended for safety assessment of existing structures with open cracks.

Declaration of Competing Interest

The author declares that he has no known competing financial interests or personal relationships that could have appeared to influence the work reported in this paper.

Data availability

Data will be made available on request.

References

[1] Cook William D, Mitchell Denis. Studies of disturbed regions near discontinuities in reinforced concrete members. Acids Struct J 1988;85(2):206–16.
[2] Schlaich Jorg, Schafer Kurt. Design and detailing of structural concrete using strut-and-tie models. Struct. Eng 1991;69(6):113–25.
[3] Desnerck Pieter, Lees Janet M, Morley Chris T. Strut-and-tie models for deteriorated reinforced concrete half-joints. Eng Struct 2018;161:41–54.
[4] Mata-Falcón Jaime, Pallarés Luis, Miguel Pedro F. Proposal and experimental validation of simplified strut-and-tie models on dapped-end beams. Eng Struct 2019;183:594–609.
[5] CEN European Committee for Standardization. Eurocode 2. Design of concrete structures Part 1–1: General rules and rules for buildings. Brussels (Belgium): EN 1992–1-1; 2004. p. 225.
[6] Desnerck Pieter, Lees Janet M, Morley Chris T. Impact of the reinforcement layout on the load capacity of reinforced concrete half-joints. Eng Struct 2016;127:227–39.
[7] Mata-Falcón, J., Serviceability and Ultimate Behaviour of Dapped-end Beams (In Spanish: Estudio del comportamiento en servicio y rotura de los apoyos a media madera). PhD Thesis, Universitat Politècnica de València; 2015.
[8] P. Kumaraguru, trength of Dapped End Beams. MSc Thesis, University of Calgary, Calgary, Alberta, Canada; 1992, 81–94.
[9] Herzinger R. Stud reinforcement in dapped ends of concrete beams. Calgary, Alberta, Canada: PhD thesis, University of Calgary; 2008. p. 139–228.
[10] Barton DL. Detailing of structural concrete dapped end beams. MSc. thesis. Austin, Texas, USA: University of Texas; 1988. p. 77–126.
[11] Rajapakse, Chathura. "Behaviour and Modelling of Reinforced Concrete Dapped-End Connections." PhD Thesis, University of Liege and Hasselt University; 2023.
[12] Rajapakse Chathura, Degée Hervé, Mihaylov Boyan. Investigation of shear and flexural failures of dapped-end connections with orthogonal reinforcement. Eng Struct 2022;260:114233.
[13] Desnerck Pieter, Lees Janet M, Morley Chris T. Strut-and-tie models for deteriorated reinforced concrete half-joints. Eng Struct 2018;161:41–54.
[14] Johnson, P.M., Couture, A. and Nicolet, R., Report of the Commission of inquiry into the collapse of a portion of the de la Concorde overpass. Government of Quebec; 2007.
[15] di Prisco M, Colombo M, Martinelli P, Coronelli D. 2018. The technical causes of the collapse of annone overpass on SS. 36. Ital Concr Days 2018:1–16.
[16] Zhu Ronnie RH, et al. Crack width prediction using compatibility-aided strut-and-tie model. Struct J 2003;100(4):413–21.
[17] Rajapakse Chathura, Degée Hervé, Mihaylov Boyan. Assessment of failure along re-entrant corner cracks in existing RC dapped-end connections. Struct Eng Int 2021;31(2):216–26.
[18] Sigrist, V., Zum. Verformungsvermögen von Stahlbetonträgern (Vol. 210). (On the Deformation Capacity of Structural Concrete Girders), ETH Zurich;1995.
[19] Engstrom, B., J. Magnusson, and Zhiyong Huang. "Pull-out bond behavior of ribbed bars in normal and high-strength concrete with various confinements." Special Publication 180 (1998): 215–242.
[20] Marti Peter, et al. Tension chord model for structural concrete. Struct Eng Int 1998;8(4):287–98.
[21] Tepfers Ralejs. Cracking of concrete cover along anchored deformed reinforcing bars. Mag Concr Res 1979;31(106):3–12.